Combining Leu-enkephalin nanomedicines with enkephalinase inhibitors: A promising painkiller strategy?

Lucas Prades
Université Paris-Saclay: Universite Paris-Saclay
Hadjer Hazam
Université Paris-Saclay: Universite Paris-Saclay
Frédéric Gobeaux
CEA Paris-Saclay Center - Fontenay-aux-Roses Site: Commissariat a l'energie atomique et aux energies alternatives Site de Fontenay-aux-Roses
Semen Yesylevskyy
Institute of Physics National Academy of Sciences of Ukraine: Institut fiziki Nacional'na akademia nauk Ukraini
Christophe Ramseyer
Université de Franche-Comté: Universite de Franche-Comte
Scander Loukil
Université Paris-Saclay: Universite Paris-Saclay
Luigi Ranieri
Université Paris-Saclay: Universite Paris-Saclay
Catherine Cailleau
Université Paris-Saclay: Universite Paris-Saclay
Philippe Sitbon
INSERM U1195: Maladies et hormones du systeme nerveux
Patrick Couvreur
patrick.couvreur@universite-paris-saclay.fr

Paris-Saclay University: Universite Paris-Saclay
Sinda Lepetre-Mouelhi
Université Paris-Saclay: Universite Paris-Saclay

Research Article

Keywords: Squalene, Nanomedicines, Enkephalinase inhibitors, Enkephalin, Pain, Analgesia

Posted Date: August 8th, 2025

DOI: https://doi.org/10.21203/rs.3.rs-7163618/v1

Version of Record: A version of this preprint was published at Drug Delivery and Translational Research on November 24th, 2025. See the published version at https://doi.org/10.1007/s13346-025-01988-5.

Abstract

This study investigates the potential of a novel nanomedicine approach relying on squalene nanoparticles of endogenous enkephalinase inhibitors (EEI) – opiorphin (OPN) and STR-324 – to alleviate pain by potentiating the action of enkephalins in vivo, in a model of acute inflammatory pain. A library of squalene-based EEI prodrugs was synthesized. These prodrugs were unable to self-assemble into nanoparticles, in contrast to the other squalenoylated prodrugs, probably due to their high hydrophilicity. By incorporating either squalenic acid (SQ) or enkephalin-squalene (LENK-SQ) prodrug as adjuvants with strong self-assembling properties, we successfully formulated nanoparticles of STR- or OPN-SQ (EEI-SQ NPs) and performed their physicochemical characterization. The analgesic efficacy of these formulations was evaluated in a carrageenan-induced pain model using the Hargreaves test to assess hyperalgesia. Nevertheless, the intravenous administration of EEI-SQ NPs caused systemic toxicity which was investigated through in vitro incubation assays. It was discovered that EEI-SQ bioconjugates exhibited strong interactions with divalent anions in physiological media, leading to nanoparticles aggregation, which was further confirmed in silico by molecular dynamics simulations. EEI-SQ NPs administered subcutaneously successfully enhanced the anti-hyperalgesic effect of LENK-SQ NPs. However, it was considered as not relevant enough regarding the observed local toxicity.

Introduction

Pain remains a significant global health challenge due to its high prevalence, serious health consequences, and the limited availability of effective and safe treatments, especially for neuropathic pain. Conditions such as arthritis, cancer, and nervous system disorders contribute to this challenge, causing considerable distress to patients.

While morphine and synthetic opioids are the most powerful and widely used painkillers in clinical practice today, their administration is often accompanied by severe adverse effects such as respiratory depression, sedation, constipation, and the development of physical and psychological dependance. These drawbacks not only limit their long-term use for chronic pain but also underscore the urgent need for alternative pain therapies that are both effective and have a reduced side effect profile. It has been stated that any new analgesic agent capable of providing pain relief similar to that of morphine but with fewer side effects would significantly improve patients' quality of life [1].

Since their identification in 1975 [2], endogenous neuropeptides such as enkephalins (ENK) have been investigated for their potential to alleviate pain with significantly fewer adverse effects compared to traditional opioids [3, 4]. Despite their promising potential, ENK face limitations in their effectiveness as analgesics due to their low metabolic stability and inability to cross biological membranes [5]. To address these issues, we have recently proposed a novel nanomedicine approach allowing the specific delivery of Leu-enkephalin (LENK) neuropeptide into inflamed tissues for pain control [6]. This study, based on the so-called "squalenoylation nanotechnology" [7], showed that the rapidly metabolized LENK may become pharmacologically efficient, owing to a simple conjugation with the natural and

biocompatible lipid squalene (SQ). Therefore, the formulation of the resulting LENK-SQ bioconjugate into nanoparticles (LENK-SQ NPs) prevented rapid plasma metabolization of LENK and conferred through peptide release a notable anti-hyperalgesic effect that lasted even longer than after the treatment with morphine, in a rat model of inflammation. *In vivo* biodistribution studies revealed that NPs precisely target inflamed tissue, where peripheral opioid receptors are overexpressed, resulting in a localized analgesic effect. They also demonstrated high efficacy in a postoperative pain model, providing long-term relief [8]. Building on this approach, the present study explores the potential of still enhancing the effect of LENK-SQ NPs, using endogenous enkephalinase inhibitors (EEIs), offering a complementary pain alleviation strategy.

Opiorphin (OPN) and its stable derivative STR-324 (STR), two endogenous pentapeptides that inhibit enkephalin-degrading enzymes, have attracted considerable attention in recent years for their potent analgesic effects comparable to those of morphine. By inhibiting metalloproteases such as aminopeptidase N (APN) and neutral endopeptidase (NEP), endogenous enkephalinase inhibitors (EEIs) were found to increase local enkephalin concentrations, enabling effective pain modulation via indirect activation of opioid receptors [9–11]. Another important advantage of using these endogenous peptides as analgesic agents is that many of the side effects associated with morphine and morphine-like drugs are absent. This is because they do not directly activate opioid receptors; instead, their mechanism of action prevents excessive stimulation of the ubiquitously distributed opioid system. Consistently, studies have shown that subchronic treatments with opiorphin do not lead to significant abuse potential, dependence, or antiperistaltic effects [12], and does not induce tolerance or cross-tolerance with morphine [9], highlighting its favorable safety profile for potential long-term use. Additionally, STR-324 has demonstrated significant analgesic efficacy in postoperative [13] and neuropathic pain models [14] following a one-week intravenous infusion, with no associated adverse effects. Notably, STR-324 is currently undergoing clinical trials for the management of postoperative pain and has already shown an excellent safety profile [15] and promising preliminary results [16].

Nevertheless, the clinical application of both opiorphin and STR-324 remains limited by their short duration of action following systemic administration, primarily due to rapid degradation by peptidases in the bloodstream [17]. The metabolic half-life of native OPN in human plasma has been estimated at approximately 5 minutes [17]. In the light of these considerations, we propose here a novel approach to potentiate the well-established analgesic effect of LENK-SQ NPs through their combination with OPN or STR. First, LENK-SQ NPs were co-administered with STR-324 to determine whether it could enhance analgesic activity in an inflammatory pain model. Subsequently, with the aim of addressing severe pain, new nanoformulations were developed to deliver STR or OPN alongside LENK precisely and efficiently to the site of pain, using the “squalenoylation” nanotechnology [7, 18]. In that respect, OPN and STR-324 were first conjugated to squalene derivative either directly or using chemical linkers, resulting in a library of EEIs squalenoylated prodrugs. These prodrugs were then formulated into nanoparticles (EEI-SQ NPs) or co-formulated with LENK-SQ prodrugs (multidrug EEI-SQ/LENK-SQ NPs). Nanoformulations were characterized, and their analgesic effect was further evaluated in a carrageenan-induced pain model using Hargreaves test to determine the most promising combination.

Materials and methods

1. Synthesis of LENK-SQ and EEI-SQ bioconjugates

1.1. Synthesis of Leu-enkephalin-squalene bioconjugate

The synthesis of the LENK-SQ bioconjugate was conducted following the protocol described by Feng et al [6]. Briefly, 1,1',2-Tris-norsqualenic acid (SQ) [500 mg, 1.25 mmol] and triethylamine (TEA) [139 mg, 1.37 mmol] were dissolved in 9 mL of anhydrous tetrahydrofuran (THF) under argon and the mixture was then cooled at 0°C prior to the dropwise addition of ethyl chloroformate [135 mg, 1.25 mmol] under stirring. The reaction mixture was then allowed to rise to room temperature and after 1 h of stirring, a solution of Leu-enkephalin (LENK) [690 mg, 1.25 mmol] solubilized in 9 mL of dimethylformamide (DMF) was added to the mixture and the reaction was kept under stirring for 72 h. The solvents were then removed under vacuum and the crude product was purified by Flash Chromatography Biotage Selekt [purification with gradient eluent DCM/EtOH (100:0 to 85:15)]. A filtration through silica column was then performed using EtOH/AcOEt (40:60) as eluent to remove the triethylammonium salt. The pure LENK-SQ bioconjugate was obtained in 54% yield.

1.2. Chemical synthesis of STR-SQ bioconjugates

1.2.1. Synthesis of squalenoyl hexamethylene diamine (SQ-HM) and squalenoyl 2.2'-(ethylenedioxy)bis(ethylamine) (SQ-PEG_2) bioconjugate intermediates

To a stirred solution of 1.1'.2-trisnorsqualenic acid (300 mg, 0.749 mmol) in anhydrous DMF (22 mL), was added under nitrogen 2-(1H-7-azabenzotriazol-1-yl)-1,1,3,3-tetramethyluronium hexafluorophosphate (HATU; 341.6 mg, 0.899 mmol), 1-hydroxybenzotriazole hydrate (HOBt; 137.6 mg, 0.899 mmol) and diisopropylethylamine (116.2 mg, 0.899 mmol). The reaction mixture was stirred 12 hours at room temperature to allow activation of the tris-nor-squalenic acid. Then, Hexamethylenediamine spacer (HM; 313.0 mg, 2.697 mmol) or 2.2'-(ethylenedioxy)bis(ethylamine) spacer (PEG_2; 399.7 mg, 2.697 mmol) was added. The reaction was left under stirring for 3 days and was then concentrated in vacuo. Aqueous sodium hydrogen carbonate was added (20 mL) and the mixture was extracted with ethyl acetate (2 × 20 mL) and dichloromethane (1 × 20 mL). The combined extracts were washed with brine, dried over $MgSO_4$, and concentrated under reduced pressure. The crude product was purified by silica gel column (DCM/EtOH gradient, 100:0 to 93:7), affording pure SQ-HM or SQ-PEG_2 intermediates in yields of 62.5% and 61%, respectively.

1.2.2. Synthesis of Squalenoyl-HM-STR (STR-HM-SQ) and Squalenoyl-PEG_2-STR (STR- PEG_2-SQ) bioconjugates

To a stirred solution of STR (230.1 mg, 0.346 mmol) in anhydrous DMF (18 mL), was added under nitrogen, 2-(1H-7-azabenzotriazol-1-yl)-1,1,3,3-tetramethyluronium hexafluorophosphate (HATU; 157.8 mg, 0.415 mmol), 1-hydroxybenzotriazole hydrate (HOBt; 63.5 mg, 0.415 mmol) and diisopropylethylamine (134.0 mg, 1.037 mmol). Then, SQ-HM intermediate (60.2 mg, 0.5187 mmol) or SQ-PEG_2 intermediate (76.8 mg, 0.5187 mmol) was added to the mixture. The reaction was left under stirring for 3 days and was then concentrated in vacuo. The crude reaction mixture was triturated with ether, and the ether supernatant containing lipophilic residues was removed. This procedure was repeated four times. After ether rinses, the crude product underwent an initial purification by silica gel column chromatography using a gradient of DCM/MeOH, starting from 100:0. A second purification was then performed using a semi-preparative reverse-phase HPLC (RP-HPLC) system (HPLC 1260 Infinity, Agilent, USA) on a Waters C18 column (4.6 × 150 mm, pore size = 5 µm) (Waters, Massachusetts, USA). RP-HPLC was performed using gradient elution with mobile phases consisting of 0.2% (v/v) TFA in water and acetonitrile (ACN). Pure SQ-HM-STR and SQ-PEG_2-STR were obtained in yields of 20% and 35%, respectively (Fig. SI-3, SI-4, SI-6, SI-7, SI-9, SI-10, SI-11).

1.3. Chemical synthesis of OPN-SQ bioconjugate:

To a stirred solution of 1,1',2-tris-nor-squalenic acid (32 mg, 0.079 mmol) in anhydrous THF (2 mL), TEA (9 mg, 0.086 mmol) was added under nitrogen. The reaction mixture was cooled to 0 °C before the addition of ethyl chloroformate (9 mg, 0.086 mmol). The mixture was then allowed to warm to room temperature and kept stirring for 1 h. A solution of opiorphin (50 mg, 0.072 mmol) in 2 mL of anhydrous DMF was then added and the reaction was stirred at room temperature for 4 days. The solvents were removed under reduced pressure and the crude product was purified. The purification was conducted on silica gel using a gradient of DCM/MeOH starting from 100:0. Total yield of the pure OPN-SQ product was 56% (Fig. SI-5, SI-8, SI-12).

2. Preparation of EEI-SQ nanoparticles

LENK-SQ NPs were prepared as previously described in references [6, 8, 19]. STR-SQ NPs and OPN-SQ NPs were prepared using the nanoprecipitation method. Briefly, the bioconjugate (either STR-HM-SQ or STR-PEG_2-SQ or OPN-SQ, 2 mg) was dissolved in pure ethanol (250 µl) in the presence of tris-nor-squalenic acid (SQ) as an adjuvant (mass ratio 1:1, ***strategy 1***) or LENK-SQ as an adjuvant (mass ratio 1:1, ***strategy 2***). The resulting solution was then added dropwise to water (or a 5% aqueous dextrose solution for *in vivo* tests, 1 mL) under constant stirring to yield a nanoparticle suspension (EtOH/aqueous solution ratio 1:4). The solution spontaneously turned turbid, displaying a Tyndall effect that confirmed the presence of nanoparticles. Ethanol was subsequently evaporated under reduced pressure using a Rotavapor (80 rpm, 40°C, 45 mbar) yielding an aqueous suspension of NPs with a final bioconjugate concentration of 2 mg/mL. Typically, the formulations ranged from 2 mg/mL for *in vitro* tests to 5 mg/mL for *in vivo* experiments.

3. Characterization of EEI-SQ nanoparticles

3.1. DLS

The mean particle diameter, polydispersity index (PdI) and zeta potential were determined at 25°C by Dynamic Light Scattering (DLS) using a Zetasizer Ultra (Malvern Panalytical). The measurements were made after 1/10 dilution of the nanoparticles' samples in milliQ water (diameter, PdI) or in 0.1 mM NaCl (zeta potential), in triplicate.

3.2. CryoTEM

The morphology of the nanoparticles (4 mg/mL) was observed by cryogenic transmission electron microscopy (cryoTEM). Drops of the solutions were deposited on copper grids covered with a holey carbon film (Quantifoil R3.5/1), previously treated with a plasma glow discharge (5 mA, 30 s). The excess liquid on the grids was blotted out with filter paper, and the grids were quickly immersed in liquid ethane to form a thin vitreous ice film. The whole process was performed using a Vitrobot apparatus (FEI Company). Observations were conducted at low temperature (-180°C) on a JEOL 2010 FEG microscope operated at 200 kV. Images were acquired with a Gatan K2 direct detection camera. Typically, a stack of 20 dose-fractionated images (0.2 s acquisition/frame with a maximum dose of 20 e-/pixel/second) were recorded and then aligned to compensate for specimen motion, drift and irradiation damage with the Gatan Microscopy Suite DigitalMicrograph.

3.3. SAXS & WAXS

Small-angle X-ray scattering patterns (SAXS) were obtained on the SWING beamline of the SOLEIL synchrotron (Saint-Aubin, France). The scattering vector range q of 0.002 to 2.5 $Å^{-1}$ was obtained with an energy of 16 keV and two sample-to-detector distances (6 and 0.50 m for the SAXS and the wide-angle X-ray scattering ranges, respectively). The data were recorded by a two-dimensional Eiger 4 M (Dectris) detector. Data reduction was performed using Foxtrot software (Xenocs). The samples were placed in 1.5-mm diameter glass capillaries sealed with wax. Typical acquisition sequence was 11 or 21 frames with acquisition time of 750 ms and 350 ms gap.

4. *In vivo* experiments

4.1. Animals

Adult male Sprague-Dawley rats (180-200 g upon arrival, 250-300 g at the time of the experiments) sourced from Janvier Labs, Le Genest Saint-Isle, France, were utilized for algesimetry tests. They were

housed in groups of three rats per cage in a room with 12 h alternating light / dark cycle (8: 00 pm / 8: 00 am) and controlled temperature (22° ± 2 °C) and hygrometry (50 ± 5 %). Food and water were available ad libitum. Behavioral tests, care and euthanasia of study animals were conducted according to the European legislation 2010/63/EU and approved by Ethical Animal Committee (APAFIS #42786-2023041414397950 and APAFIS #34379-2021121514291649).

4.2. Carrageenan-induced paw edema model

The carrageenan-induced paw edema model is a widely accepted acute inflammation model for screening compounds with anti-inflammatory potential [20]. Practically, λ-Carrageenan was freshly prepared by dissolving it in physiological saline (0.9% NaCl) at a concentration of 2% w/v prior to injection. Rats received a single intraplantar injection of the λ-carrageenan solution (100µL) into the plantar region of the left hind paw [21, 22] to induce inflammation. Inflammation peaked at 5 hours post-λ-carrageenan injection, at which thermal nociceptive test was performed on the ipsilateral inflamed hind paw.

4.3. Nociceptive behavioral study in rats

Thermal Nociceptive Test: Hypersensitivity to thermal nociceptive stimuli was assessed using the Hargreaves test using a plantar analgesia meter (Ugo Basile, Bioseb, Milano, Italy) [21]. Rats were individually placed in a clear plastic chamber (18 cm×29 cm×12.5cm) on an elevated transparent glass table and allowed to habituate for at least 5 minutes prior to testing. A moveable radiant heat source was positioned beneath the glass floor directly under the plantar surface of the left hind paw. The time (in seconds) from the activation of the radiant heat source to the withdrawal of the paw was measured automatically. A cut-off time of 20 seconds was set to prevent tissue damage. Each trial was repeated three times at 5-minute intervals. The average paw withdrawal latencies (PWL) were calculated and expressed as mean values ± SEM (standard error of the mean) for the curves.

Experimental design: All experiments were performed by an investigator blinded to the administered drug, and animals were acclimatized to the experimental environment 2 weeks before measurements**.** Baseline responses to thermal stimuli were obtained on the day preceding the λ-carrageenan injection. Based on prior studies, acute pharmacological treatments were administered intravenously (i.v.) 5 hours post-carrageenan injection, after the peak of the inflammatory response. The efficacy of these treatments on thermal hyperalgesia was assessed by measuring paw withdrawal latencies (PWL) using the Hargreaves test at regular intervals following drug or vehicle administration, starting at 20 minutes, then at 40 minutes and then every 30 minutes over a period of 4 h (Fig. SI-1). For subcutaneous administration of EEI-SQ NPs, the injection was performed 2 h before intravenous administration of LENK-SQ NPs, corresponding to 3 h after carrageenan injection (Fig. SI-2). Practically, a single intravenous dose of LENK-SQ NPs (20 mg/kg, eq. to 11,48 mg/kg of LENK), STR peptide (in aqueous solution, 2 mg/kg), or control solution (5% dextrose solution) was administered, based on a

LENK-SQ NP concentration of 5 mg/mL. A single subcutaneous dose of STR-HM-SQ/SQ NPs (20 mg/kg, eq. to 11,69 mg/kg of STR) was also administered.

5. *In vitro* stability of EEI-SQ NPs

To assess the potential risk of NPs aggregation *in vivo*, several formulations (4 mg/mL in water) were incubated at 37°C under agitation in various physiological media (ratio 1:3): 0,9% NaCl, Phosphate buffer saline (PBS), Fetal bovine serum (FBS), and plasma (from Sprague Dawley rats). The NPs integrity was assessed both visually and by DLS, at predefined times (5; 15; 30; 60 min), after 1/10 sample dilution. 50 µl of NPs in plasma were taken out of the Eppendorf and diluted into 450 µl of water, then measured by DLS. Blank measurements of plasma diluted 1/10 in water were done as control.

6. *In silico* molecular modeling of OPN-SQ conjugates

The molecular model of opiorphin-squalene (OPN-SQ) was built using the following procedure. **(1)** The folded conformer of opiorphin was generated by PEP-FOLD3 server [23]. The Gromacs topology for the peptide was generated by the standard Gromacs tools [24] using CHARMM36 force field [25]. **(2)** The squalene topology was generated by CHARMM-GUI ligand builder module [26, 27]. **(3)** Peptide and squalene topologies and coordinate files were combined using the custom Python script implemented with Pteros and MolAR molecular modeling libraries [28–30]. **(4**) Missing bonded interaction terms for the linkage were transferred from CHARMM-GUI output for a minimal molecular fragment representing a linkage moiety.

After that, the simulations of spontaneous OPN-SQ aggregation in aqueous solution with two different sets of ions were performed. 30 OPN-SQ conjugates were placed randomly into a cubic simulation box with the box size of 70 nm. The box was filled with ~9300 TIP3P water molecules. Then, either NaCl or Na_2HPO_4 solutions were modeled by adding 92 Cl^- or 100 HPO_4^{2-} ions and neutralizing the system with the corresponding amount of Na+ counterions. The topology of HPO_4^{2-} divalent anion was generated by CHARMM-GUI ligand builder.

Both systems were subject to energy minimizations and free MD simulations in the NPT ensemble at the temperature of 303 K and pressure of 1 bar maintained by v-rescale thermostat [31] and Parrinello-Rahman barostat [32] respectively, with the cutoff parameters recommended for CHARMM36 force field. The integration step of 2 fs was used with the bonds to hydrogen atoms turned to rigid constraints and maintained by LINCS algorithm [33]. The systems were simulated for 200 ns each. Resulting trajectories were analyzed by Gromacs analysis tools and the custom scripts based on Pteros molecular modeling library.

The radius of gyration is a measure used to describe the size or "compactness" of a collection of particles or a molecule. It is commonly employed in physics, chemistry, and biology to analyze systems

such as molecular aggregates, polymers, or proteins. The gyration radius corresponds to the average distance between the atoms or molecules in a system and their center of mass. It thus reflects how matter is distributed in space around this center. It provides insights into the compactness of a structure and changes in conformation. Tracking the evolution of the gyration radius over time allows to observe how a structure deforms or assembles.

Results

1. Analgesic efficacy of LENK-SQ NPs in combination with STR-324 via intravenous route

To assess whether the presence of an EEI could potentiate the analgesic activity of LENK-SQ NPs, we co-administered these nanoparticles intravenously with STR-324, selected for its greater chemical stability than OPN [13]. If this approach proves effective, OPN will be tested in a second phase. Baseline measurements of paw withdrawal latencies (PWL) were recorded prior to carrageenan injection, with no significant differences observed between groups (mean value ± SD of 9,86 ± 0,21 s (n=17)). At the 5 hours post-injection time point, corresponding to the peak of the inflammatory response, the mean paw withdrawal latency (PWL) was 4.78 ± 0.15 s (n = 17), reflecting a 51% reduction compared to baseline values in naïve rats (P < 0.0001; see Fig. 1).

1.1. Effect of LENK-SQ NPs on thermal hyperalgesia

The anti-hyperalgesic effect of LENK-SQ NPs (20 mg/kg) was evaluated over 4 h post-administration. As previously demonstrated [6], rats treated with LENK-SQ NPs displayed a significant reduction in thermal hyperalgesia, reflected by an increase in PWL that peaked at 40 min with a value of 7,585 ± 0,48 s (Fig. 1A). The anti-hyperalgesic effect was significant from 20 to 70 min (P<0,0001 at 20, 40 and 70 minutes compared to dextrose solution), which corresponded to the previously described LENK-SQ NPs performances [6].

1.2. Effect of STR peptide on thermal hyperalgesia

The effect of acute treatment with 2 mg/kg of STR-324 administered intravenously was comparable to that of the dextrose solution at all time points (P>0,9999) (Fig. 1A). Accordingly, no statistically significant difference was observed in the AUC of STR-324 compared to that of the dextrose solution (Fig. 1B). STR-324 alone did not exhibit any antinociceptive effect in the anti-inflammatory pain model, although the selected dose was based on findings from previous studies [9, 13, 14, 34].

1.3. Effect of the co-administration of STR and LENK-SQ NPs on thermal hyperalgesia

The ability of STR-324 to enhance the analgesic effect of LENK-SQ NPs by inhibiting LENK degradation was assessed through co-administration with LENK-SQ NPs. This combination significantly reversed the effect of carrageenan at 20-, 40- and 70-minutes post administration (P<0,0001 vs. dextrose solution). However, no significant differences were observed between the co-treatment and the treatment with LENK-SQ NPs alone, either in terms of intensity or duration of action at any time point (P=0,1068 at 20 minutes, P>0,9999 at 40 and 70 minutes) (Fig. 1A). These results were confirmed by examination of values of AUC (Fig. 1B). Consequently, no potentiation mediated by STR-324 to enhance the analgesic efficacy of LENK-SQ NPs was observed. This was likely due to the rapid degradation of STR-324 by peptidases in the bloodstream.

2. Synthesis of the EEI-SQ conjugates

To further investigate the potential analgesic effect of OPN or STR-324, which are inhibitors of the enkephalin-degrading enzymes NEP and APN, a second approach was developed to protect them from rapid degradation. This strategy involved converting these molecules into prodrugs and formulating them as nanoparticles, with the goal of increasing their local concentration at the site of pain. This targeted delivery approach has already proven effective for the fragile LENK neuropeptide, enabling a potent analgesic effect by delivering it directly to the site of pain. The prodrug strategy was subsequently applied to these EEIs by conjugating a squalene moiety to the N-terminal site of OPN (Fig. 2A) or to the C-terminal site of STR-324 (Fig. 2B) using two different spacers.

2.1. Synthesis of STR-SQ bioconjugates

The STR-SQ conjugate was obtained by coupling the tris-nor-squalenic acid to the C-terminal of STR-324, using two diamine C_6 spacers with different sensitivity to hydrolysis in order to modulate the release kinetics of STR from NPs: 2.2'-(ethylenedioxy)bis(ethylamine) (diamino PEG_2) and hexamethylenediamine (HM). First, tris-nor-squalenic acid was activated using HATU and HOBt prior being coupled to the PEG_2 spacer or HM spacer. Then, the resulting SQ-PEG_2 or SQ-HM were conjugated using the same approach to the C-terminal site of the STR-324 peptide. The STR-HM-SQ (Fig. 2D, SI-3, SI-6) and STR-PEG_2-SQ (Fig. 2E, SI-4, SI-7) were obtained with total yields of 12,5% and 21,5% yield, respectively.

2.2. Synthesis of OPN-SQ bioconjugate

Since opiorphin is an unstable peptide whose N-terminal glutamine readily cyclizes into pyroglutamate to form STR-324, squalenoylation was performed directly on the amino group of OPN. Consequently, the OPN-SQ conjugate (Fig. 2C) was synthesized by directly coupling squalenic acid to the N-terminal amine group of the OPN peptide. To achieve this, squalenic acid was first activated into its mixed anhydride

using ethyl chloroformate, which was then reacted with OPN, resulting in the OPN-SQ conjugate with a yield of 56% (Fig. SI-5, SI-8).

3. Formulation of EEI-SQ NPs

Upon synthesis, the nanoprecipitation method was employed to assess the nano-assembly capability of these EEI-SQ bioconjugates. This method involved dissolving the bioconjugates in ethanol and adding the ethanolic solution dropwise to an aqueous phase. However, none of these bioconjugates successfully formed nanoparticles using this approach. Furthermore, thebioconjugates exhibited relative solubility in water, likely due to the highly hydrophilic nature of the OPN and STR peptides. This outcome was particularly intriguing, as other highly hydrophilic squalenoylated conjugates, such as siRNA, have demonstrated self-assembling properties despite their hydrophilic nature [35]. Moreover, the presence of positively charged arginine residues may induce repulsion between the bioconjugate molecules, thus hindering their nanoassembly and potentially accounting for the failure of the nanoprecipitation process.

To further investigate the observed phenomenon, the ClogP values of the bioconjugates were first calculated. ClogP is a computational metric used to predict the hydrophobicity or hydrophilicity of compounds. A ClogP value close to 0 or negative indicates a hydrophilic molecule, while higher ClogP values correspond to increased hydrophobicity. The calculated ClogP values were 4.99 for STR-HM-SQ, 4.17 for STR-PEG_2-SQ, and 3.93 for OPN-SQ (Fig. SI-12). For comparison, the ClogP value of LENK-SQ was 11.53, and other self-assembling squalene bioconjugates typically exhibit average ClogP values around 10 (Ad-SQ: 10.17, gemcitabine-SQ: 9.6, Doxorubicin-SQ: 11,04). These values emphasized the significantly greater hydrophilicity of the OPN and STR bioconjugates, likely attributed to the arginine residues of the peptides.

Another critical chemical parameter is the hydrophilic-lipophilic balance (HLB). A low HLB value indicates a more lipophilic molecule. In the study by Coppens et al. [36], squalenoylated gemcitabine and other lipidic bioconjugates were compared to assess their ability to self-assemble into nanoparticles. The HLB was identified as a reliable predictor of nanoparticle self-assembly. The authors demonstrated that nanoparticles exhibited self-assembly properties when the HLB value of the bioconjugate was below 7.45, while a value above 9 prevented this phenomenon. For the tested EEI-SQ bioconjugates, HLB values were 9.85, 11.07, and 10.13, for STR-HM-SQ, STR-PEG_2-SQ, and OPN-SQ, respectively, while HLB value of LENK-SQ was only 7.60 (Fig. SI-12). These findings provide a credible explanation for the failure of the EEI-SQ bioconjugates to self-assemble into nanoparticles.

To achieve the goal of formulating EEI-SQ into nanoparticles, the inclusion of adjuvants in the formulation was subsequently considered.

3.1. Nanoformulation of EEI-SQ bioconjugates

A typical approach to enhance nanoprecipitation is the addition of surfactants like Pluronic F68 or Tween 80; however, this method was found ineffective in this case. In that respect, tris-nor-squalenic acid (SQ) was considered for its excellent self-assembly properties and its ability to form effective stacking with the squalene moiety of EEI bioconjugates. Initial formulations containing 5% to 40% w/w of SQ resulted in highly unstable and non-reproducible NPs formulations. Optimal formulation was achieved with 50% w/w EEI-SQ/SQ using the nanoprecipitation method, providing the most stable NPs (***strategy 1***).

A second strategy focused on using the LENK-SQ bioconjugate as an adjuvant. This approach served a dual purpose: first, to promote nanoassembly through interactions between squalene moieties of both bioconjugates (ie., LENK-SQ and EEI-SQ) , and second, to generate hybrid nanoparticles capable of providing a dual analgesic effect by co-releasing LENK and EEI (***strategy 2***). Thus, hybrid nanoparticles were obtained through the co-nanoprecipitation of EEI-SQ and LENK-SQ bioconjugates (1:1 w/w ratio).

4. Characterization of EEI-SQ NPs using DLS

Dynamic light scattering (DLS) measurements of the various EEI-SQ nanoformulations revealed an average size close to 100 nm for all nanoparticles and a positive surface charge (Table 1). EEI-SQ nanoparticles formulated with squalenic acid alone exhibited high zeta potentials, typically ranging from +50 mV to +60 mV, suggesting the likely exposure of arginine residues on their surface. In contrast, control SQ nanoparticles and LENK-SQ nanoparticles, which both exposed carboxylic acid groups on their surface, produced negatively charged nanoparticles.

Hybrid EEI-SQ/LENK-SQ nanoparticles exhibited a lower positive zeta potential of around +35 mV, suggesting that the exposed carboxylic acid group of LENK moiety partially neutralized the positive charges contributed by the arginine residues of EEI moiety on the nanoparticle surface. In the case of EEI-SQ with squalenic acid as the adjuvant, the small carboxylic acid group was likely shielded, preventing it from counterbalancing the positive charges of EEI and resulting in a higher overall zeta potential.

Table 1: Formulations and characterization of EEI-SQ NPs from strategy 1 (*adjuvant: SQ; 1/1 w/w*) and strategy 2 (*adjuvant: LENK-SQ 1/1: w/w*). *The colored boxes in the table (orange, yellow, purple, black, blue, and green) represent specific formulations and are used consistently in the subsequent figures to enable easy comparison between table and figures.*

	STR-HM-SQ NPs		STR-PEG$_2$-SQ NPs		OPN-SQ NPs	
Adjuvant	SQ	LENK-SQ	SQ	LENK-SQ	SQ	LENK-SQ
Size (nm)	100 ± 19	92 ± 10	87 ± 2	90 ± 7	87 ± 3	92 ± 3
PDI	0.145	0.121	0.154	0.083	0.215	0.175
Zeta Potential (mV)	+60 ± 10	+35 ± 5	+50 ± 10	+34 ± 6	+55 ± 4	+35 ± 3

4.1. Structural characterization of EEI-SQ NPs using cryoTEM, SAXS & WAXS

4.1.1. Comparative study of STR-PEG_2-SQ NPs and STR-HM-SQ NPs using SQ as adjuvant

This section focuses on the influence of the linker on the morphology and structure of the nanoparticles. The morphology of the nanoparticles was analyzed by cryoTEM. Fig. 3A-B shows images of STR-HM-SQ NPs/SQ (strategy 1), with nanoparticles revealing spherical shapes with sizes ranging from 30 to 100 nm (see size distribution in Fig. 3C). The discrepancy between diameter measurements obtained by DLS (100±19 nm) and cryoTEM (56 ±20 nm) was attributed to differences related to the hydrodynamic radius, as previously described [37]. However, the most striking—and surprising—feature is the coexistence of these nanoparticles with fiber-like structures. This will be further described and commented on in the following section.

In contrast, STR-PEG_2-SQ/SQ formulations produced only nanoparticles (without fibers) with a broader size distribution ranging from 20 to 140 nm (Fig. 3D-F). These nanoparticles exhibited a faceted shape and a distinctive internal multilayer structure, with a layer thickness of 4.9 nm (Fig. 3G-H). While STR-HM-SQ/SQ NPs did not exhibit a specific organized structure (Fig. 3B), STR-PEG_2-SQ/SQ NPs displayed a lamellar organization (Fig. 3E,G,H). This structural difference was attributed to a bilayer stiffening induced by the hydrophilic PEG_2 linker which generates thicker hydrophilic domains resulting in the formation of more linear architectures. Although STR-PEG_2-SQ nanoparticles displayed a more organized internal structure, they exhibited reduced colloidal stability, an observation that reflects the absence of a direct relationship between internal structural order and colloidal stability.

Given that STR-PEG_2-SQ nanoparticles appeared less stable over time, as compared to STR-HM-SQ and OPN-SQ, these studies primarily focused on the latter two types of nanoparticles. Indeed, STR-PEG_2-SQ nanoparticles precipitated within the first two days. While their higher HLB suggests a reduced propensity for self-assembly compared to the other bioconjugates, self-assembly capacity alone did not fully explain their colloidal instability, as no direct relationship necessarily exists between these two properties.

4.1.2. Comparative study between OPN-SQ NPs and STR-HM-SQ NPs using SQ and LENK-SQ as adjuvants

In-depth physicochemical studies were conducted to better understand the structure of OPN-SQ NPs and STR-HM-SQ NPs. Thus, four nanoformulations composed of OPN-SQ and SQ-HM-STR, each combined with either SQ or LENK-SQ as adjuvant, were characterized using cryoTEM observations and SAXS-WAXS analyses. A typical image of each formulation is displayed in Fig. 3 (panels I to L). The Fig. 3I and 3J highlight the coexistence, here again, of nanoparticles in the 50-90 nm range (see size

statistics in Table SI-2) and micrometer-long, possibly millimeter-long fibers, when either STR-HM-SQ or OPN-SQ was formulated with SQ using the nanoprecipitation method.

More pictures of these fibers are displayed in Fig. SI-13 and show that the morphology of the fibers differed depending on the bioconjugate. Indeed, STR-HM-SQ/SQ fibrils appeared better defined and possibly slightly more rigid if we rely on their apparent persistence length. Their diameter was on the order of 50 nm (Fig. SI-13C); by contrast, the OPN-SQ/SQ fibers had a less consistent diameter that could reach up to 100 nm (Fig. SI-13G-H). These fibers coexisted with less well-defined nanoparticles (see blue arrows in Fig. SI-13G) than the NPs observed in STR-HM-SQ/SQ (Fig. 3B and I). In any case, subfibrillar structures approximately 5-7 nm in diameter could be observed (Fig. SI-13 D-E & H-I).

When STR-HM-SQ and OPN-SQ were co-nanoprecipitated with LENK-SQ, they formed more typical spherical nanoassemblies (Fig. 3K and 3L, respectively) with diameters ranging from 64 ± 25 nm to 92 ± 28 nm (Table SI-2). These values are consistent with those generally expected for squalene-based nanoparticles. No trend or correlation could be found to explain these differences.

The same EEI-SQ NPs suspensions were also characterized by small- and wide-angle x-ray scattering (SAXS-WAXS) experiments performed on the SWING beamline at the SOLEIL Synchrotron (Saint-Aubin, France). The corresponding curves are plotted in Fig. 4. For comparison purposes, the curves corresponding to SQ-COOH NPs or LENK-SQ NPs (nanoformulations of adjuvants alone) are represented in SI (Fig. SI-14).

As described above, the two formulations of STR-HM-SQ (with SQ and LENK-SQ as adjuvants) exhibited very different morphologies, which was confirmed by the SAXS profiles (Fig. 4A). The WAXS patterns, however, exhibited a peak at the same position (q_{max} = 0.13 $Å^{-1}$) (Fig. 4B). This could suggest that the two STR-HM-SQ shared a similar nanostructure; however, given that the peak for STR-HM-SQ/SQ (containing fibers and spheres) was smaller than that of STR-HM-SQ/LENK-SQ (containing only spheres), this peak was most likely the signature of these spheres and did not correspond to fibers (Fig. 4B). The position of these peaks indicated the existence of a characteristic length $d = 2\pi/q_{max}$ = 5 nm, that could be related to the dimension of the water channels in a sponge phase (Table SI-3). Noteworthy, on the cryoTEM images of the STR-PEG_2-SQ NPs (similar bioconjugate, but with a more hydrophilic PEG_2 linker forming only spheres), a 4.9 nm period was measured between the layers observed in the spherical NPs (see Fig. 3G-H). For STR-HM-SQ, the full width at half-maximum (FWHM) reflects the correlation length $\xi = 2\pi/FWHM$, representing the distance over which these characteristic lengths are correlated: 19.9 nm with SQ versus 13.5 nm with LENK-SQ (Table SI-3).

Overall, it is difficult to draw definitive conclusions from this set of observations. We can nonetheless mention that when SQ was used as an adjuvant, the nano-assemblies exhibited polymorphism as fibers were observed along with the more “classical” spherical NPs. This suggests that there might be a segregation of the two bioconjugates. The two morphologies would reflect different compositions. We hypothesize that the spherical NPs would mostly contain SQ (as pure SQ-COOH form spherical NPs),

while the fibers would be mostly constituted of STR-HM-SQ. By contrast, when LENK-SQ was used as an adjuvant, only spherical NPs were formed, which suggests that the two bioconjugates are evenly distributed in the nano-assemblies.

We further hypothesize that the different behaviors induced by the two adjuvants is related to their respective sizes: while LENK, OPN and STR are all peptides and, when conjugated to squalene, result in similar amphiphilic structures (LENK-SQ, OPN-SQ, STR-SQ), SQ itself is much smaller, with its hydrophilic moiety limited to a carboxylic group. It was then concluded that LENK-SQ is a more effective structuring adjuvant than plain SQ.

As for the inner structure of these nano-assemblies, all the STR-SQ formulations displayed a characteristic length of ~5 nm, suggesting a similar packing driven by the STR peptide. When OPN was used, either a larger length (6.6 nm) was measured or no structure, suggesting that OPN had a more labile and less structuring behavior than STR.

5. Evaluation of the analgesic efficacy of STR-HM-SQ NPs

The pharmacological activity of EEI-SQ NPs was evaluated starting with STR-HM-SQ/SQ NPs (strategy 1) before testing the combination STR-HM-SQ/LENK-SQ NPs (strategy 2), notably because the first formulation was more stable. The analgesic activity of STR-HM-SQ/SQ NPs administered intravenously at a dose of 20 mg/kg was evaluated using the carrageenan-induced pain model, as described previously. The experiment was conducted according to the same timeline as presented in Supplementary Information (Fig. SI-2). Moreover, since STR-HM-SQ prodrug itself is water-soluble, it was also tested at 20 mg/kg to allow comparison between its nanoparticulate and soluble forms.

However, a high mortality rate among rats was observed within minutes after administration of STR-HM-SQ, regardless of whether it was injected as soluble prodrug form or as nanoparticles when nanoprecipitated with SQ. All animals developed an acute and severe systemic reaction within seconds of administration. Symptoms included cyanosis, hypoxia, sedation, severe respiratory distress, paraplegia and cardiac arrest, leading in some cases to death (Fig. SI-16).

These symptoms suggested several potential medical conditions, such as pulmonary or vascular embolism, or an acute reaction consistent with CARPA (Complement Activation-Related Pseudoallergy) [38].

In a parallel experiment, other formulations, including OPN-SQ/SQ NPs, and hybrid nanoparticles containing both STR-HM-SQ and LENK-SQ bioconjugates, exhibited similar signs of toxicity and/or mortality. In contrast, rats treated with soluble STR peptide free didn’t show any symptom.

6. *In vitro* behavior of STR-HM-SQ NPs in biological media

To better understand the *in vivo* toxicity observed after the intravenous administration of STR-HM-SQ/SQ NPs or STR-HM-SQ soluble prodrug, *in vitro* incubation tests were conducted in various biological media. Initial tests in rat plasma showed that STR-HM-SQ soluble prodrug resulted in intense aggregation, leading to immediate gelling of the sample. STR-HM-SQ/SQ NPs exhibited rapid aggregation too, as measurable by DLS and visible to the naked eye (Fig. SI-17), supporting the hypothesis of pulmonary embolism. A similar behavior was observed when the nanoparticles were incubated in fetal bovine serum (FBS), suggesting that plasma proteins might play a role in the aggregation process.

To distinguish if proteins were (or not) responsible for the aggregation, the nanoparticles were placed in less complex physiological media. When incubated in phosphate-buffered saline (PBS), significant aggregation was observed, too. This result was consistent whether STR-HM-SQ was in its free bioconjugate form or formulated as nanoparticles. However, no aggregation was detected when the nanoparticles were incubated in physiological saline (0.9% NaCl) (Table 2).

Table 2: Summary of in vitro tests. Prodrug or nanoparticle formulations were incubated in biological or buffered media.

Incubation medium	Prodrug STR-HM-SQ	STR-HM-SQ NPs
Rat plasma	Aggregation	Aggregation
Fetal Bovine Serum	Aggregation	Aggregation
Phosphate Buffer Saline	Aggregation	Aggregation
NaCl 0,9%	No aggregation	No aggregation

These findings indicated that proteins were unlikely the primary contributor to the aggregation phenomenon, suggesting a probable ionic interaction between the divalent negatively charged phosphate ions and the positively charged guanidinium groups of the arginine residues in STR at physiological pH. Concretely, divalent anions, such as disodium phosphate (Na_2HPO_4), which are present in PBS, FBS, and plasma, but not NaCl 0.9%, could potentially chelate two arginine residues from two distinct STR-HM-SQ bioconjugates. Moreover, this behavior was consistent with the same observations made with STR-PEG_2-SQ and OPN-SQ formulations. Of note, OPN or STR free peptides never exhibited such aggregation issues. This implies that the presence of the squalene lipid moiety linked to the peptides fostered the precipitation of the chelation complex.

To confirm the likely chelation of STR bioconjugates by divalent anions, molecular modelling studies were further conducted.

7. Molecular modeling of the OPN-SQ interaction with ions

We investigated how OPN-SQ molecules interacted with each other in different saline solutions in order to determine how these interactions may influence their physical properties, such as their ability to aggregate and to form specific spatial structures. We employed a computational model of OPN-SQ aggregation (*see Materials and Methods*) using two types of salts (NaCl or Na_2HPO_4 based on the previously observed *in vitro* results).

A quick aggregation of OPN-SQ conjugates was observed within the first 20-30 ns of simulations in both ionic solutions; however, the structures of the aggregates were very different. In NaCl solution compact spherical aggregates, which diffused freely in the simulation box, were formed (Fig. 5A). In contrast, in Na_2HPO_4 solution, the aggregates were loose and highly irregular spanning the whole simulation box and creating a rigid network that interacted with their own periodic images (Fig. 5B).

Pronounced difference in the kinetics of aggregate formation and their size was apparent from the evolution of their gyration radii shown in Fig. 5C. The aggregates in NaCl solution quickly relaxed to a very stable constant gyration radius of ~1.9 nm, while in Na_2HPO_4 solution the minimal gyration radius reached only ~3 nm and fluctuated randomly due to constant jumps of the monomers of non-compact aggregates across the periodic boundaries of the simulation box.

We have also computed the effective diffusion coefficients of OPN-SQ conjugates during the first ~10 ns of simulations when no stable aggregates were formed yet. The mean square displacement method was used as implemented in the “gms msd” tool. In the NaCl solution the diffusion coefficient of conjugates was $D = 0.044 \pm 0.008 \times 10^{-5}$ cm^2/s, while in the Na_2HPO_4 solution it was almost two times smaller $D = 0.023 \pm 0.003 \times 10^{-5}$ cm^2/s. Slower diffusion of conjugates in Na_2HPO_4 solution likely resulted from the very rapid formation of dimers and larger oligomers of OPN-SQ molecules, which were cross-linked by the HPO_4^{2-} divalent anions.

Overall, molecular simulation data indicated that early stages of spontaneous aggregation of OPN-SQ conjugates depended significantly on the ionic composition of the solution. In NaCl solution, compact freely diffusing aggregates were formed, while in Na_2HPO_4 solution OPN-SQ were cross-linked by HPO_4^{2-} divalent anions so heavily that they form an extended diffuse network-like structure. Although it was not possible to extrapolate this early-stage aggregation behavior directly into the macroscopic behavior of OPN-SQ solutions, it provides possible evidence of eager formation of the gel-like phase in media containing Na_2HPO_4.

8. Evaluation of the analgesic efficacy of STR-HM-SQ nanoparticles following subcutaneous administration

8.1. Effect of the co-administration of STR-HM-SQ NPs (s.c.) and LENK-SQ NPs (i.v.) on thermal hyperalgesia

To overcome the side effects resulting from the intravenous administration of STR-HM-SQ/SQ NPs, and with the aim of enhancing the analgesic activity of LENK-SQ NPs intravenously injected (i.v.), the subcutaneous (s.c.) route of administration was chosen for the administration of STR-HM-SQ/SQ NPs. Thus, this combined administration of LENK-SQ NPs (i.v.) and STR-HM-SQ/SQ NPs (s.c.) was evaluated in the carrageenan-induced paw edema model in rats using the Hargreaves test to assess the anti-hyperalgesic pharmacological activity. Baseline PWLs were measured prior to carrageenan injection and at the peak of inflammation (3 hours post-injection). Immediately afterward, STR-HM-SQ/SQ NPs were administered (s.c., 20 mg/kg), followed by LENK-SQ NPs (i.v., 20 mg/kg) 2 hours later, to allow the STR-HM-SQ NPs or bioconjugate to reach the bloodstream via the lymphatic pathway (aligning with the timing of LENK-SQ NPs). PWLs were recorded at various time points before and after treatments, as outlined in Supplementary Information.

Baseline values, measured before carrageenan injection, remained stable for at least 2 days and did not differ between groups. Carrageenan induced significant thermal hyperalgesia in all groups (P<0,0001) (Fig. 6A). When administered alone, LENK-SQ NPs significantly increased the PWLs until 70 minutes post-administration (P<0,0001 at 20, 40 and 70 minutes), with a maximum effect at 40 min (P<0,0001 vs. dextrose solution. The combination of LENK-SQ NPs (iv) with STR-HM SQ/SQ NPs (s.c.) produced a comparable overall reduction in thermal hyperalgesia lasting until 70 minutes post-administration (P<0,0001 vs. dextrose solution), with a significantly enhanced antinociceptive effect observed at 20 minutes, compared to LENK-SQ NPs alone (P=0,003). Specifically, the combined treatment increased the PWL to 8.8 ± 0.7 s, compared to 7.3 ± 0.6 s with LENK-SQ NPs alone (Fig. 9A). In contrast, STR-HM-SQ/SQ NPs alone did not exhibit any analgesic effect, as shown by the absence of any increase in PWL during the 2 hours following their subcutaneous injection (P > 0.9999).

Meanwhile, the group treated with both LENK-SQ NPs and the free STR peptide from the previous experiment reached its higher anti-nociceptive effect at 20 minutes too (8,2± 0,6 s, as shown in Fig. 1 and 6A).

Based on the AUC analysis (Fig. 6B), the co-treatment of STR-HM-SQ/SQ NPs (s.c.) and LENK-SQ NPs (i.v.) resulted in a 35% increase in the overall analgesic effect, as compared to LENK-SQ NPs alone. Overall, the combination of the two treatments did not extend the duration of the analgesia, as compared to LENK-SQ NPs (iv) but enhanced intensity.

8.2. Local site toxicity observations

The subcutaneous administration of STR-HM-SQ/SQ NPs did not result in acute toxicity signs, such as hypoxia, observed after intravenous administration and no animals died in this group. However, the subcutaneous administration led to a local toxicity related to the formation of a cyst at the injection site, averaging 1 cm in size (Fig. SI-18), which became visible 72 hours post injection. This could explain the limited efficacy of STR-HM-SQ/SQ NPs for improving the anti-nociceptive activity of LENK-SQ NPs, as

observed in Fig. 6; likely, only a small fraction of STR-HM-SQ/SQ NPs were able to diffuse, while the majority remained trapped under the skin, forming the observed cyst.

Discussion

In previous studies, we demonstrated the potential of LENK-SQ NPs for managing acute inflammatory pain [6] and post-operative pain [8]. Building on this, we propose here a novel approach to potentiate the effects of LENK-SQ NPs by using an additional treatment based on endogenous enkephalinase inhibitors, such as opiorphin and its stable derivative STR-324. To the best of our knowledge, while Chaillet et al. potentiated the analgesic effect of intracerebroventricular injection of Met-enkephalin using synthetic dual enkephalinase inhibitors *(DENKIs)* in the 1980s [39], the present study is the first to adopt a peripheral administration route.

To ensure consistency and allow comparison with previous studies with LENK-SQ NPs, we chose to assess the potentiation of enkephalins by EEIs using the same inflammatory pain model. Our findings demonstrated that the anti-hyperalgesic effect of LENK-SQ NPs was not significantly enhanced through the co-administration of STR-324 – likely due to its short half-life – since the administration of STR-324 alone did not produce any anti-hyperalgesic effect.

In an attempt to extend the analgesic activity of LENK-SQ NPs, we applied the previously described “squalenoylation” technology [7, 18] to the EEIs in order to increase their *in vivo* half-life and to promote their accumulation within inflamed tissues, as has been previously demonstrated with LENK-SQ NPs [6]. Thus, a library of squalenoylated bioconjugates of STR-324 and opiorphin was synthesized by coupling squalene derivatives either directly via an amide bond or through a biocleavable spacer, allowing the modulation of EEI release. Interestingly, unlike typical squalene derivatives, these squalene bioconjugates failed to self-assemble into nanoparticles using the standard nanoprecipitation method, likely due to their high overall hydrophilicity. To address this challenge, we exploited the self-assembling properties of squalene by co-formulating these EEIs with a squalene-derived adjuvant, either tris-nor-squalenic acid (SQ) or LENK-SQ bioconjugate. Beyond its role as a formulation adjuvant, the LENK-SQ bioconjugate was expected to exert a synergistic or additive effect with the EEIs, potentially enhancing the pharmacological efficacy in terms of duration and intensity.

The characterization of EEIs-SQ revealed positively charged nanoparticles, likely due to the arginine residues in the EEIs peptides, with a hydrodynamic diameter of around 100 nm. CryoTEM analysis further indicated that the nature of the linker significantly influenced the nanoparticle structure and morphology. While the lipophilic HM linker favored the formation of spherical STR-HM-SQ/SQ nanoparticles, the hydrophilic PEG_2 linker induced faceted shapes with a more organized internal lamellar structure in STR-PEG_2-SQ/SQ NPs. These observations align with findings previously observed with LENK-SQ bioconjugates [19] where it was demonstrated that the linker could significantly influence nanoparticle internal structure. A study conducted by Lepeltier et al. [40], which examined how the

chemical structure of squalene bioconjugates affects nanoparticle architecture, further supports this direction.

Furthermore, the choice of adjuvants used in the nanoformulations also impacted the nanoparticles. For instance, the addition of SQ led to fibers formation, whereas adding LENK-SQ did not produce such fibers. The impact of these fibers and their overall effects remains to be further explored and better understood. Indeed, squalene nanoparticles fibers have been described previously by Mougin et al. [41] where it was demonstrated that squalenoyl-doxorubicin (SQ-Dox) conjugate formed elongated nanoparticles with improved therapeutic efficacy and decreased toxicity compared to free doxorubicin [41, 42].

However, LENK-SQ addition caused instability in formulations, likely due to the strong local ionic pairing between positively charged EEI-SQ and LENK-SQ bioconjugates which are likely negatively charged at physiological pH. Despite the overall positive surface charge of + 35 mV, this local charge neutralization at the particle interface can disrupt repulsive electrostatic interactions, leading to aggregation and loss of colloidal stability. For example, OPN-SQ/LENK-SQ NPs rapidly flocculated and appeared to fuse (*see Fig. SI-15 in supplementary information*). Conversely, the STR-HM-SQ/SQ NPs formulation was stable and was therefore selected for further *in vivo* testing.

Surprisingly, STR-HM-SQ/SQ NPs administered intravenously to rats in a model of acute inflammatory pain, demonstrated systemic toxicity, which led to the rapid death of a significant number of animals. Numerous examples concerning the toxicity of positively charged nanoparticles have been reported in the literature, with cationic lipidic nanoparticles (LNPs) being the most significant. Excessive cationic charge in LNPs induces dose-dependent toxicity, including hepatotoxicity and pulmonary inflammation [43–45]. Additionally, interactions with erythrocytes, can result in hemolysis [46]. Cationic lipids are also known to activate the complement system, leading to hemodynamic disturbances and rapid clearance by macrophages of the reticuloendothelial system [43, 45]. Nonetheless, this current study constitutes the first report describing squalenoyl conjugates nanoparticles exhibiting such deleterious behavior.

In vitro studies revealed intense aggregation of the nanoparticles when incubated in plasma, serum, or PBS, but not in NaCl. These findings suggested that divalent ions, such as Na_2HPO_4, might mediate aggregation by forming cross-links between bioconjugates of two different nanoparticles. Molecular modeling confirmed this hypothesis. It is likely that the interaction between the squalene bioconjugates and ions triggered rapid and intense aggregation *in vivo*, leading to the observed pulmonary embolism.

To mitigate systemic toxicity, subcutaneous injection was proposed as an alternative administration route. Thus, we evaluated the subcutaneous administration of STR-HM-SQ/SQ NPs in combination with the intravenous injection of LENK-SQ NPs. This approach resulted in a slight but significant enhancement of the analgesic activity but did not achieve the expected prolongation. Furthermore, we observed a local toxicity with the formation of a cyst at the subcutaneous injection site.

Conclusion

This study introduces an innovative approach for the design, synthesis and characterization of nanoparticles composed of endogenous enkephalinase inhibitors (EEI-SQ) aimed at enhancing the analgesic effect of leu-enkephalin–squalene nanoparticles (LENK-SQ NPs) by reducing enzymatic degradation. Intravenous administration of EEI-SQ NPs led to systemic toxicity, likely linked to filament formation, as suggested by *in vitro* physico-chemical investigations and in silico analyses. Subcutaneous injection of STR-HM-SQ/SQ NPs co-administered with LENK-SQ NPs (i.v.) moderately enhanced the analgesic effect compared to LENK-SQ NPs (i.v.) alone; however, local toxicity was observed at the subcutaneous injection site. Current investigations aim to better understand this toxicity through advanced molecular modelling and detailed physico-chemical characterization (SAXS, WAXS, cryoTEM). In particular, the contribution of strong positive surface charges to nanoparticle aggregation and local toxicity is being explored, with strategies such as grafting lipophilic moieties or using anionic surfactants to modulate surface properties. These mitigation strategies aim to overcome the identified challenges and ultimately improve the safety and efficacy of these multifunctional nanoparticles. Overall, this study provides valuable insights into the potential of EEI-SQ NPs to enhance the anti-hyperalgesic activity of LENK-SQ NPs and highlights the promise of combining antinociceptive enkephalins with enkephalinase inhibitors for effective pain relief.

Declarations

Contributions

Lucas Prades is the main author of this article and participated to the design of the studies, performed the experiments and wrote the sections on chemical synthesis, nanoparticles formulation and characterization under the supervision of Sinda Lepetre-Mouelhi, with the assistance of two master's students (Luigi Ranieri and Scander Loukil). Hadjer Hazam participate to the design of the *in vivo* study, conducted the behavioral experiments and wrote the section of behavior studies under the supervision of Philippe Sitbon. Patrick Couvreur discussed the planned experiments and the data. The SAXS/WAXS and cryoTEM physicochemical characterization was conducted and written by Frédéric Gobeaux in collaboration with Lucas Prades and Sinda Lepetre-Mouelhi. Catherine Cailleau participated to the design and the realization of behavioral experiment. Data are formatted and written by Lucas Prades and Hadjer Hazam. Molecular modeling was conceptualized by Semen Yesylevskyy and Christophe Ramseyer. Simulations were performed, analyzed and described by Semen Yesylevskyy. Simulation results were interpreted by Semen Yesylevskyy, Christophe Ramseyer, Lucas Prades and Sinda Lepetre-Mouelhi. This manuscript was written by Lucas Prades and Hadjer Hazam, reviewed by Sinda Lepetre-Mouelhi, Philippe Sitbon and Patrick Couvreur. All authors reviewed and approved the final version of the manuscript.

Fundings

This research was supported by a grant from the French Agency for Research (Agence Nationale de la Recherche) under AAPG2021 NANOPAINKILL project, and as part of France 2030 program ANR-11-IDEX-0003, awarded by the Graduate School of Chemistry of the Université Paris-Saclay.

Ethical approval

Behavioral tests, care and euthanasia of study animals were conducted according to the European legislation 2010/63/EU and approved by Ethical Animal Committee (APAFIS #42786-2023041414397950 and APAFIS #34379-2021121514291649). Animal models are among the most crucial in vivo models concerning basic parameters like Nociceptive behavioral studies, as these pre-clinical data are essential before translating into humans.

Conflict of interest

All authors (L. Prades, H. Hazam, F. Gobeaux, S. Yesylevskyy, C. Ramseyer, L. Ranieri, S. Loukil, Philippe Sitbon, P. Couvreur, S. Lepetre-Mouelhi) declare that they have no confict of interest.

Consent to participate

All the authors approved the participation.

Consent for publication

All the authors approved the publication of the manuscript.

Data availability

The datasets generated during and/or analysed during the current study are available from the corresponding author on reasonable request.

References

1. McQuay H. Opioids in pain management. Lancet. 1999;353:2229–32. doi:10.1016/S0140-6736(99)03528-X.
2. Hughes J, Smith TW, Kosterlitz HW, Fothergill LA, Morgan BA, Morris HR. Identification of two related pentapeptides from the brain with potent opiate agonist activity. Nature. 1975;258:577–80. doi:10.1038/258577a0.
3. Pradhan AA, Befort K, Nozaki C, Gavériaux-Ruff C, Kieffer BL. The delta opioid receptor: an evolving target for the treatment of brain disorders. Trends Pharmacol Sci. 2011;32:581–90.

doi:10.1016/j.tips.2011.06.008.

4. Hohenwarter L, Böttger R, Li S-D. Modification and Delivery of Enkephalins for Pain Modulation. Int J Pharm. 2023;646:123425. doi:10.1016/j.ijpharm.2023.123425.
5. Schwartz JC, Malfroy B, La Baume S de. Biological inactivation of enkephalins and the role of enkephalin-dipeptidyl-carboxypeptidase ("enkephalinase") as neuropeptidase. Life Sci. 1981;29:1715–40. doi:10.1016/0024-3205(81)90182-X.
6. Feng J, Lepetre-Mouelhi S, Gautier A, Mura S, Cailleau C, Coudore F, et al. A new painkiller nanomedicine to bypass the blood-brain barrier and the use of morphine. Sci Adv. 2019;5:eaau5148. doi:10.1126/sciadv.aau5148.
7. Couvreur P, Stella B, Reddy LH, Hillaireau H, Dubernet C, Desmaële D, et al. Squalenoyl nanomedicines as potential therapeutics. Nano Lett. 2006;6:2544–8. doi:10.1021/nl061942q.
8. Hazam H, Prades L, Cailleau C, Mougin J, Feng J, Benhamou D, et al. A nanomedicine approach for the treatment of long-lasting pain. J Control Release. 2024;373:688–98. doi:10.1016/j.jconrel.2024.07.033.
9. Rougeot C, Robert F, Menz L, Bisson J-F, Messaoudi M. Systemically active human opiorphin is a potent yet non-addictive analgesic without drug tolerance effects. J Physiol Pharmacol. 2010;61:483–90.
10. Wisner A, Dufour E, Messaoudi M, Nejdi A, Marcel A, Ungeheuer M-N, Rougeot C. Human Opiorphin, a natural antinociceptive modulator of opioid-dependent pathways. Proc Natl Acad Sci U S A. 2006;103:17979–84. doi:10.1073/pnas.0605865103.
11. Tian X, Chen J, Xiong W, He T, Chen Q. Effects and underlying mechanisms of human opiorphin on colonic motility and nociception in mice. Peptides. 2009;30:1348–54. doi:10.1016/j.peptides.2009.04.002.
12. Popik P, Kamysz E, Kreczko J, Wróbel M. Human opiorphin: the lack of physiological dependence, tolerance to antinociceptive effects and abuse liability in laboratory mice. Behav Brain Res. 2010;213:88–93. doi:10.1016/j.bbr.2010.04.045.
13. Sitbon P, van Elstraete A, Hamdi L, Juarez-Perez V, Mazoit J-X, Benhamou D, Rougeot C. STR-324, a Stable Analog of Opiorphin, Causes Analgesia in Postoperative Pain by Activating Endogenous Opioid Receptor-dependent Pathways. Anesthesiology. 2016;125:1017–29. doi:10.1097/ALN.0000000000001320.
14. van Elstraete A, Sitbon P, Hamdi L, Juarez-Perez V, Mazoit J-X, Benhamou D, Rougeot C. The Opiorphin Analog STR-324 Decreases Sensory Hypersensitivity in a Rat Model of Neuropathic Pain. Anesth Analg. 2018;126:2102–11. doi:10.1213/ANE.0000000000002413.
15. Moss LM, Berends CL, van Brummelen EMJ, Kamerling IMC, Klaassen ES, Bergmann K, et al. First-in-human trial to assess the safety, tolerability, pharmacokinetics and pharmacodynamics of STR-324, a dual enkephalinase inhibitor for pain management. Br J Clin Pharmacol. 2022;88:103–14. doi:10.1111/bcp.14931.

16. van Dasselaar T, van der Wal I, van Velzen M, Juarez-Perez V, Sitbon P, Dahan A. Influence of STR-324, a Dual Enkephalinase Inhibitor, on Postoperative Pain Scores: A Proof-of-Concept Trial in Patients after Laparoscopic Surgery. Anesthesiology. 2024;140:632–3. doi:10.1097/ALN.0000000000004864.
17. Bogeas A, et al. Structure- Activity Relationship Study and Function-Based Petidomimetic Design of Human Opiorphin with Improved Bioavailability Property and Unaltered Analgesic Activity. Biochem & Pharmacol 2013. doi:10.4172/2167-0501.1000122.
18. Feng J, Lepetre-Mouelhi S, Couvreur P. Design, Preparation and Characterization of Modular Squalene-based Nanosystems for Controlled Drug Release. Curr Top Med Chem 2017. doi:10.2174/1568026617666170719171728.
19. Lepetre-Mouelhi S, Gobeaux F, Da Silva A, Prades L, Feng J, Wien F, et al. Leu-Enkephalin Lipid Prodrug Nanoparticles: Relationship between Nanoparticles' Structure, Interaction with Bovine Serum Albumin, and Analgesic Activity. Chem. Mater. 2024;36:694–707. doi:10.1021/acs.chemmater.3c02070.
20. Winter CA, Risley EA, Nuss GW. ANTI-INFLAMMATORY AND ANTIPYRETIC ACTIVITIES OF INDO-METHACIN, 1-(p-CHLOROBENZOYL)-5-METHOXY-2-METHYL-INDOLE-3-ACETIC ACID. The Journal of Pharmacology and Experimental Therapeutics. 1963;141:369–76. doi:10.1016/S0022-3565(25)26625-3.
21. Hargreaves K, Dubner R, Brown F, Flores C, Joris J. A new and sensitive method for measuring thermal nociception in cutaneous hyperalgesia. Pain. 1988;32:77–88. doi:10.1016/0304-3959(88)90026-7.
22. Meller ST, Cummings CP, Traub RJ, Gebhart GF. The role of nitric oxide in the development and maintenance of the hyperalgesia produced by intraplantar injection of carrageenan in the rat. Neuroscience. 1994;60:367–74. doi:10.1016/0306-4522(94)90250-x.
23. Lamiable A, Thévenet P, Rey J, Vavrusa M, Derreumaux P, Tufféry P. PEP-FOLD3: faster de novo structure prediction for linear peptides in solution and in complex. Nucleic Acids Res. 2016;44:W449-54. doi:10.1093/nar/gkw329.
24. Abraham MJ, Murtola T, Schulz R, Páll S, Smith JC, Hess B, Lindahl E. GROMACS: High performance molecular simulations through multi-level parallelism from laptops to supercomputers. SoftwareX. 2015;1-2:19–25. doi:10.1016/j.softx.2015.06.001.
25. Huang Y-W, Cambre M, Lee H-J. The Toxicity of Nanoparticles Depends on Multiple Molecular and Physicochemical Mechanisms. Int J Mol Sci 2017. doi:10.3390/ijms18122702.
26. Lee J, Cheng X, Swails JM, Yeom MS, Eastman PK, Lemkul JA, et al. CHARMM-GUI Input Generator for NAMD, GROMACS, AMBER, OpenMM, and CHARMM/OpenMM Simulations Using the CHARMM36 Additive Force Field. J Chem Theory Comput. 2016;12:405–13. doi:10.1021/acs.jctc.5b00935.
27. Jo S, Kim T, Iyer VG, Im W. CHARMM-GUI: a web-based graphical user interface for CHARMM. J Comput Chem. 2008;29:1859–65. doi:10.1002/jcc.20945.

28. Yesylevskyy SO. Pteros: fast and easy to use open-source C++ library for molecular analysis. J Comput Chem. 2012;33:1632–6. doi:10.1002/jcc.22989.
29. Yesylevskyy SO. Pteros 2.0: Evolution of the fast parallel molecular analysis library for C++ and python. J Comput Chem. 2015;36:1480–8. doi:10.1002/jcc.23943.
30. Yesylevskyy S. MolAR: Memory-Safe Library for Analysis of MD Simulations Written in Rust. J. Comput. Chem. 2025;46:e27536. doi:10.1002/jcc.27536.
31. Bussi G, Donadio D, Parrinello M. Canonical sampling through velocity rescaling. J Chem Phys. 2007;126:14101. doi:10.1063/1.2408420.
32. Parrinello M, Rahman A. Polymorphic transitions in single crystals: A new molecular dynamics method. Journal of Applied Physics. 1981;52:7182–90. doi:10.1063/1.328693.
33. Hess B, Bekker H, Berendsen HJC, Fraaije JGEM. LINCS: A linear constraint solver for molecular simulations. J. Comput. Chem. 1997;18:1463–72. doi:10.1002/(SICI)1096-987X(199709)18:12<1463::AID-JCC4>3.0.CO;2-H.
34. Javelot H, Messaoudi M, Garnier S, Rougeot C. Human opiorphin is a naturally occurring antidepressant acting selectively on enkephalin-dependent delta-opioid pathways. J Physiol Pharmacol. 2010;61:355–62.
35. Raouane M, Desmaele D, Gilbert-Sirieix M, Gueutin C, Zouhiri F, Bourgaux C, et al. Synthesis, characterization, and in vivo delivery of siRNA-squalene nanoparticles targeting fusion oncogene in papillary thyroid carcinoma. J Med Chem. 2011;54:4067–76. doi:10.1021/jm2000272.
36. Coppens E, Desmaële D, Naret T, Garcia-Argote S, Feuillastre S, Pieters G, et al. Gemcitabine lipid prodrug nanoparticles: Switching the lipid moiety and changing the fate in the bloodstream. Int J Pharm. 2021;609:121076. doi:10.1016/j.ijpharm.2021.121076.
37. Chernyshev VS, Rachamadugu R, Tseng YH, Belnap DM, Jia Y, Branch KJ, et al. Size and shape characterization of hydrated and desiccated exosomes. Anal Bioanal Chem. 2015;407:3285–301. doi:10.1007/s00216-015-8535-3.
38. Neun BW, Ilinskaya AN, Dobrovolskaia MA. Analysis of Complement Activation by Nanoparticles. Methods Mol Biol. 2018;1682:149–60. doi:10.1007/978-1-4939-7352-1_13.
39. Chaillet P, Marçais-Collado H, Costentin J, Yi CC, La Baume S de, Schwartz JC. Inhibition of enkephalin metabolism by, and antinociceptive activity of, bestatin, an aminopeptidase inhibitor. Eur J Pharmacol. 1983;86:329–36. doi:10.1016/0014-2999(83)90181-4.
40. Lepeltier E, Bourgaux C, Rosilio V, Poupaert JH, Meneau F, Zouhiri F, et al. Self-assembly of squalene-based nucleolipids: relating the chemical structure of the bioconjugates to the architecture of the nanoparticles. Langmuir. 2013;29:14795–803. doi:10.1021/la403338y.
41. Mougin J, Yesylevskyy SO, Bourgaux C, Chapron D, Michel J-P, Dosio F, et al. Stacking as a Key Property for Creating Nanoparticles with Tunable Shape: The Case of Squalenoyl-Doxorubicin. ACS Nano. 2019;13:12870–9. doi:10.1021/acsnano.9b05303.
42. Maksimenko A, Dosio F, Mougin J, Ferrero A, Wack S, Reddy LH, et al. A unique squalenoylated and nonpegylated doxorubicin nanomedicine with systemic long-circulating properties and anticancer

activity. Proc Natl Acad Sci U S A. 2014;111:E217-26. doi:10.1073/pnas.1313459110.

43. Ozpolat B, Sood AK, Lopez-Berestein G. Liposomal siRNA nanocarriers for cancer therapy. Adv Drug Deliv Rev. 2014;66:110–6. doi:10.1016/j.addr.2013.12.008.
44. Lee J-M, Yoon T-J, Cho Y-S. Recent developments in nanoparticle-based siRNA delivery for cancer therapy. Biomed Res Int. 2013;2013:782041. doi:10.1155/2013/782041.
45. Zhang J, Li X, Huang L. Non-viral nanocarriers for siRNA delivery in breast cancer. J Control Release. 2014;190:440–50. doi:10.1016/j.jconrel.2014.05.037.
46. Buyens K, Smedt SC de, Braeckmans K, Demeester J, Peeters L, van Grunsven LA, et al. Liposome based systems for systemic siRNA delivery: stability in blood sets the requirements for optimal carrier design. J Control Release. 2012;158:362–70. doi:10.1016/j.jconrel.2011.10.009.

Figures

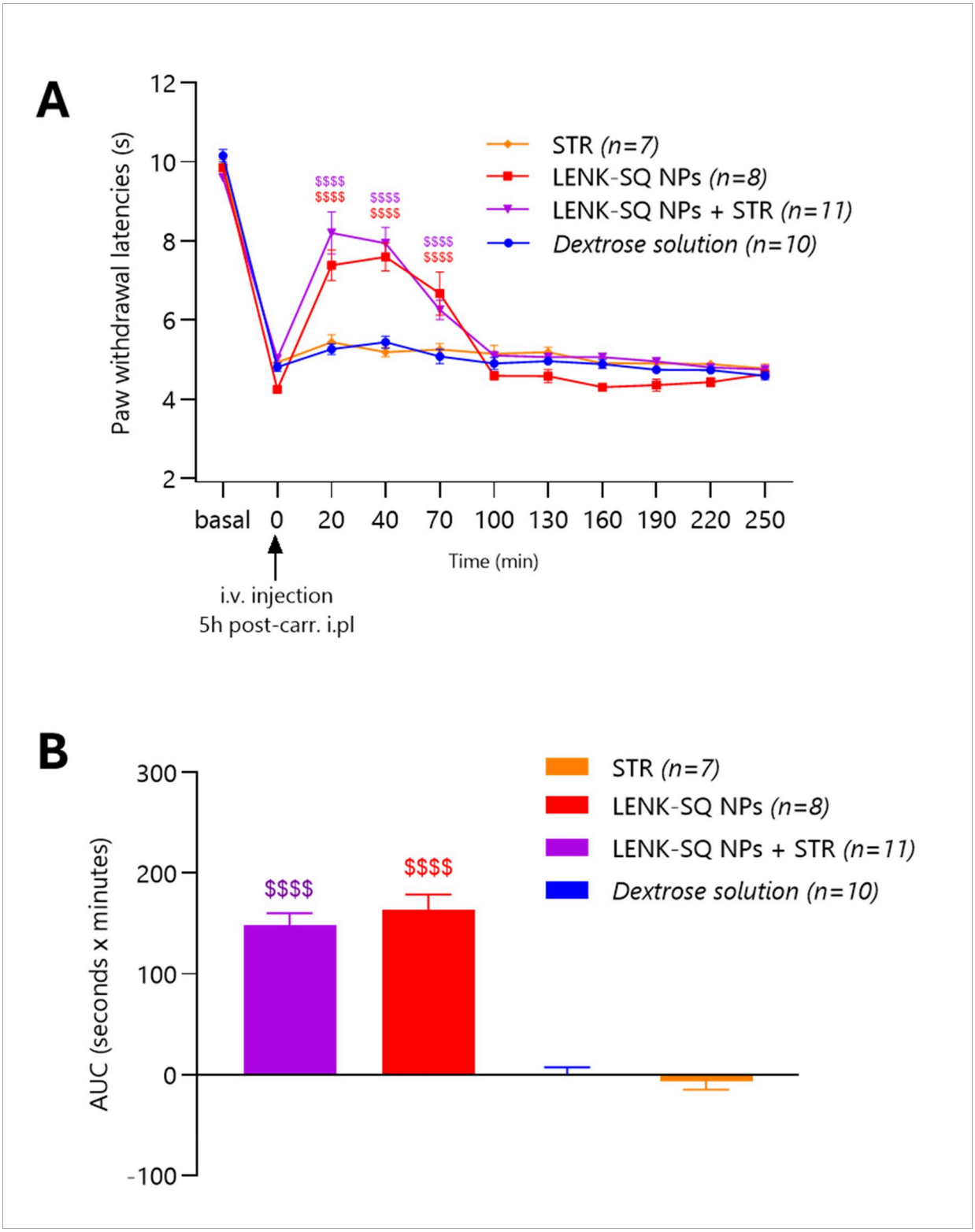

Figure 1

Behavioral effects of treatments in the carrageenan-induced inflammatory pain model. (A) Time course of the anti-hyperalgesic effects following the intravenous administration of STR-324, LENK-SQ NPs, the combination LENK-SQ NPs with STR-324, or vehicle (dextrose solution). Paw withdrawal latency (PWL) in response to the Hargreaves heat stimulus over time. Data are expressed as mean ±SEM, in seconds. Treatments were administered intravenously (at time 0 indicated by the arrow on the x-axis), 5 hours

after carrageenan injection into the left hind paw. LENK-SQ NPs and the combination of LENK-SQ NPs with STR-324 significantly increased PWL, with similar intensity and duration of action, as compared to STR-324 alone or dextrose solution,

P<0.0001, vs. dextrose solution. Two-way analysis of variance (ANOVA) with repeated measures, Bonferroni post-test. **(B) Quantification of the anti-hyperalgesic effects based on the area under the curve (AUC) analysis.** Bars are the means ± SEM of AUCs (seconds x minutes) of the cumulative durations derived from the time course changes in PWL after the various treatments.

P<0.0001; compared to dextrose solution or STR. One-way ANOVA, Tukey post-test.

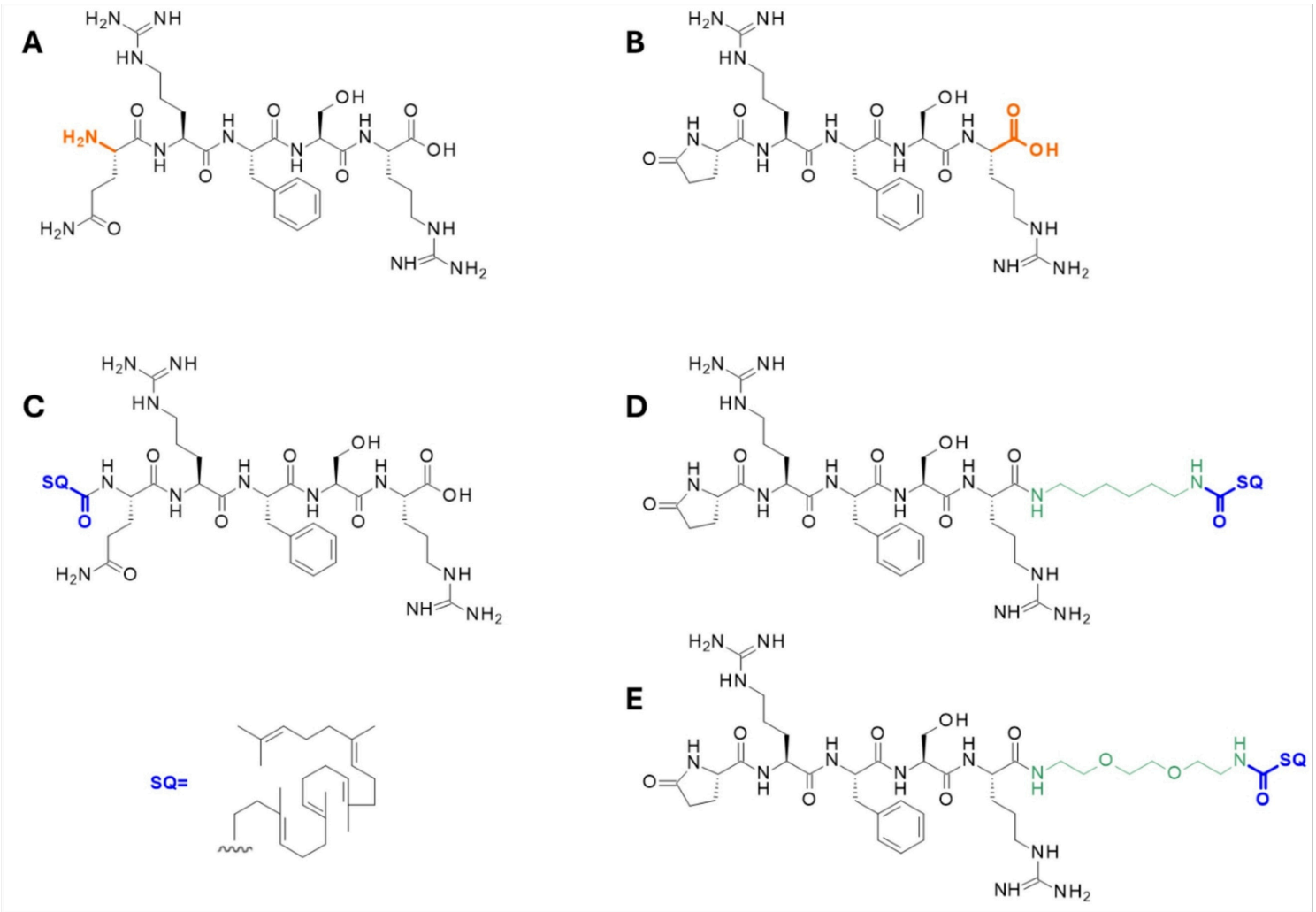

Figure 2

Chemical structures of opiorphin **(A)** and STR-324 **(B)** with their linkage sites highlighted in orange; Opiorphin-squalene conjugate with an amide linker (OPN-SQ) **(C)**; STR-squalene conjugate with a hexamethylenediamine linker (STR-HM-SQ) **(D)** and with a 2.2'-(ethylenedioxy)bis(ethylamine) linker (STR-PEG_2-SQ) **(E).** Squalene is represented in blue, linkers in green, peptides in black.

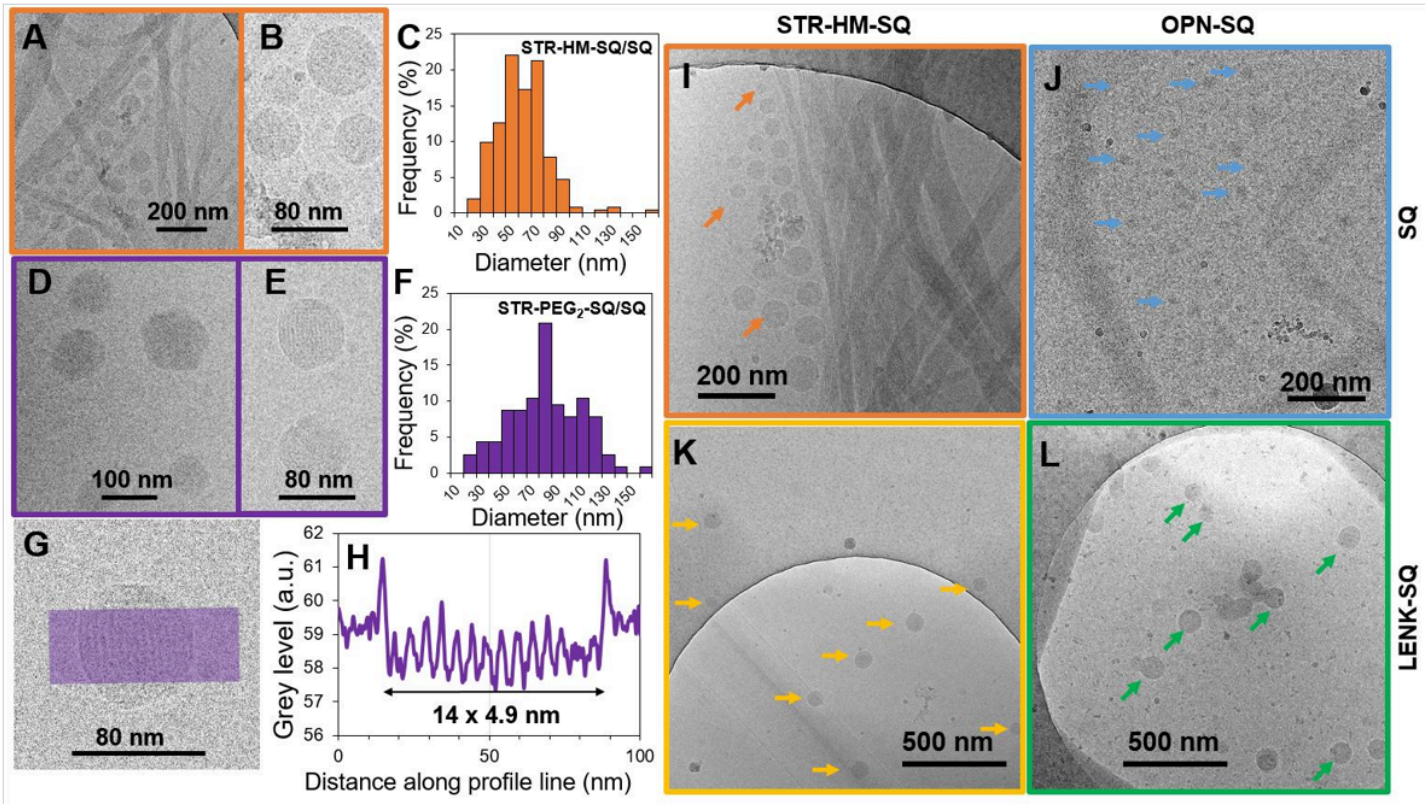

Figure 3

EEI-SQ NPs characterization. (A) Representative cryoTEM image showing spherical STR-HM-SQ/SQ NPs and fibers. **(B)** Magnified view showing the spherical NPs. **(C)** Size distribution obtained from the measurements of 254 NPs on cryoTEM images. Mean size ± SD: 56±20 nm. **(D)** Representative cryoTEM image showing faceted STR-PEG_2-SQ/SQ NPs. **(E)** Magnified view showing faceted shape and multilayer substructure. **(F)** Size distribution () obtained from the measurements of 115 NPs on cryoTEM images. Mean diameter ± SD: 76±30 nm. **(G-H)** Intensity plot profile of the inner structure of STR-PEG_2-SQ/SQ NPs. Darker grey indicates lower signal intensity. The interlayer period is 4.9 nm. **(I-L)** cryoTEM observations of EEI-SQ NPs suspensions: **(I)** STR-HM-SQ/SQ **(J)** OPN-SQ/SQ **(K)** STR-HM-SQ/LENK-SQ **(L)** OPN-SQ/LENK-SQ. Colored arrows point towards some of the nanoparticles.

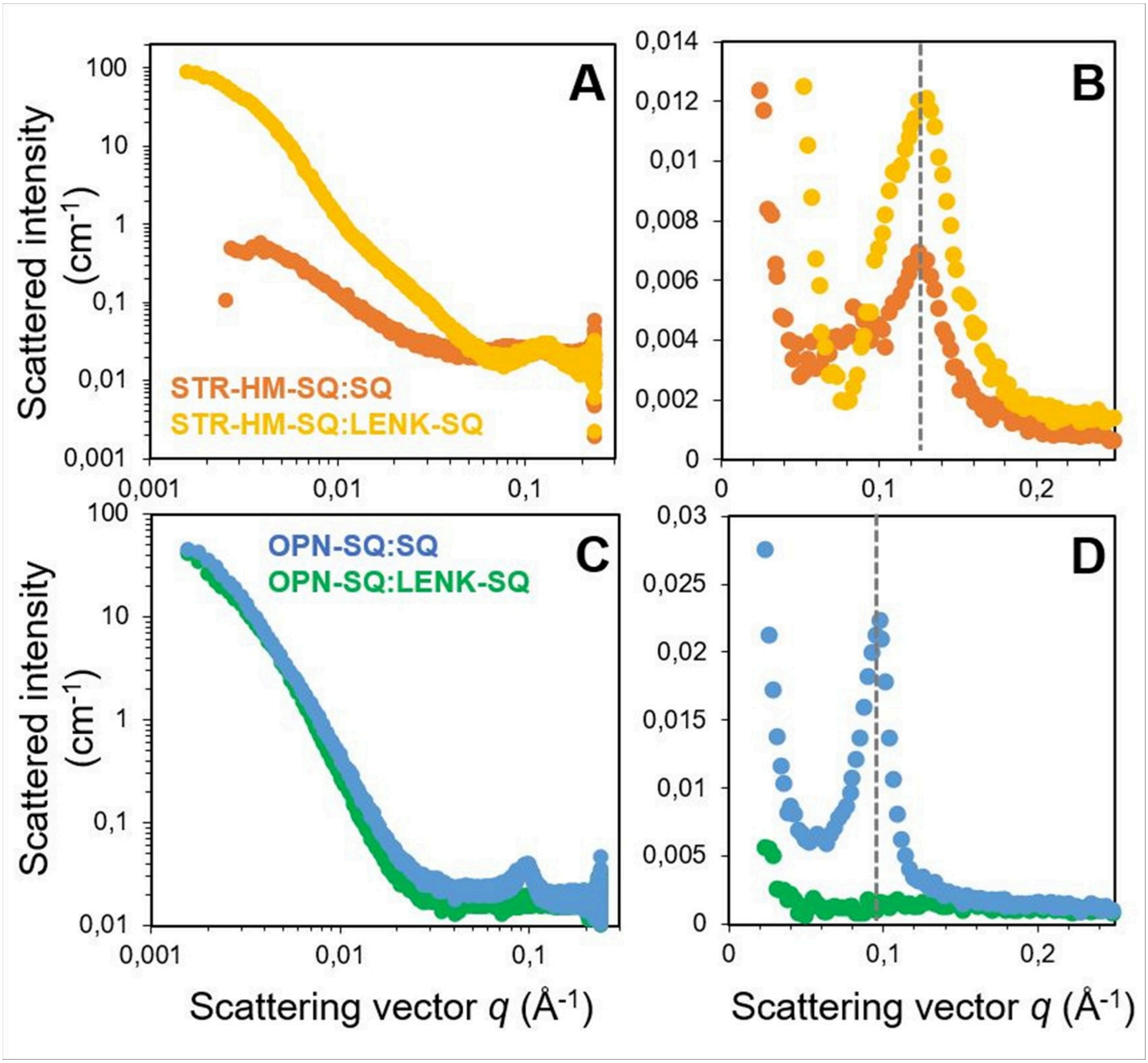

Figure 4

SAXS and WAXS patterns of HM-STR-SQ (**A-B**) and OPN-SQ (**C-D**) with either SQ or LENK-SQ adjuvant. The dashed grey lines indicate the position of the q_{max} of the WAXS structure peak.

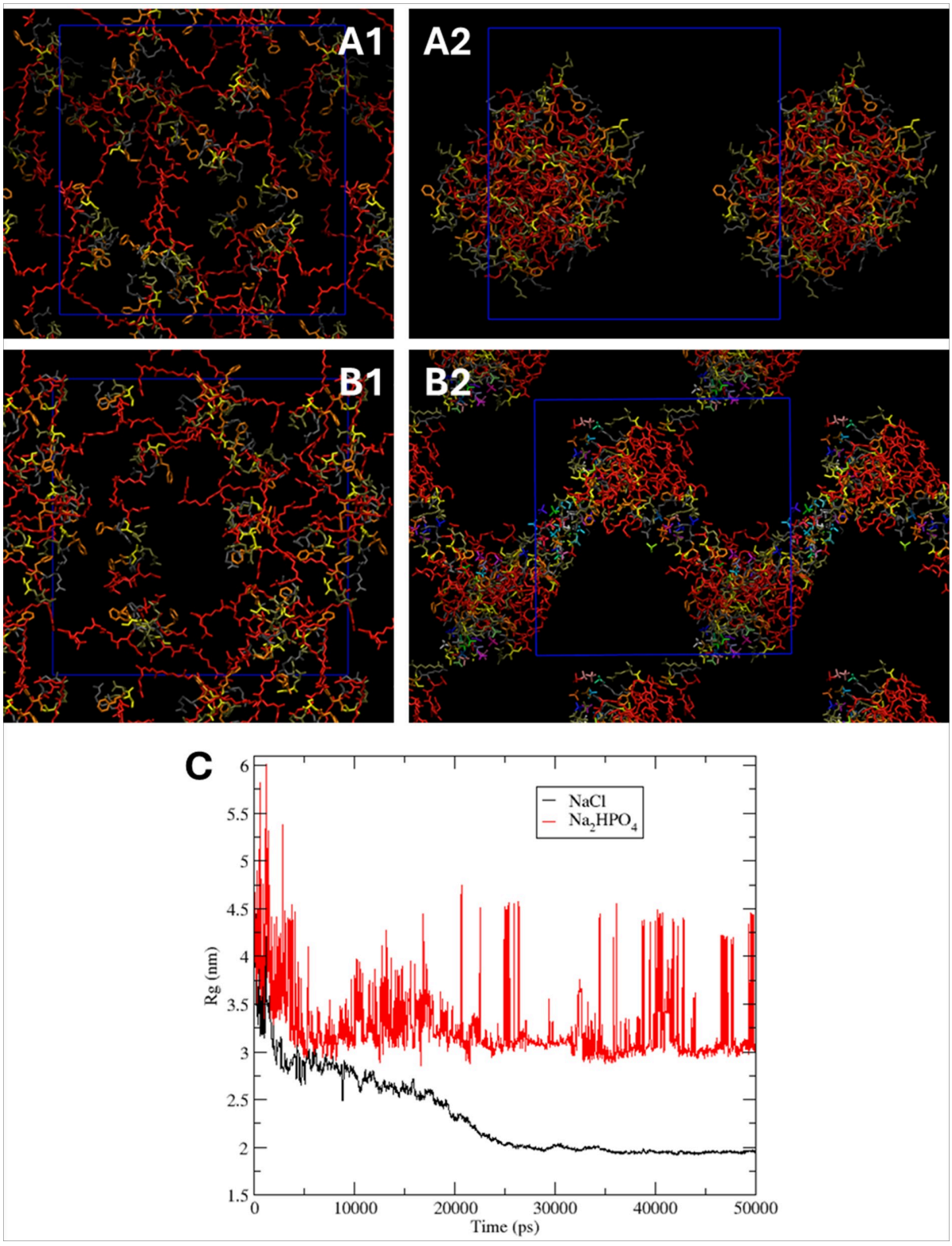

Figure 5

A) Initial (A1) and final (A2) states of the system with 30 OPN-SQ in NaCl solution.
B): Initial (B1) and final (B2) states of the system with 30 OPN-SQ in Na_2HPO_4 solution.

For both A) and B), squalene moiety is shown in red, OPN residues in yellow and shades of orange, and the simulation box in blue. Several periodic images of the systems are shown for clarity.

C): Evolution of the radius of gyration of the system with 30 OPN-SQ in NaCl and Na_2HPO_4 solutions.

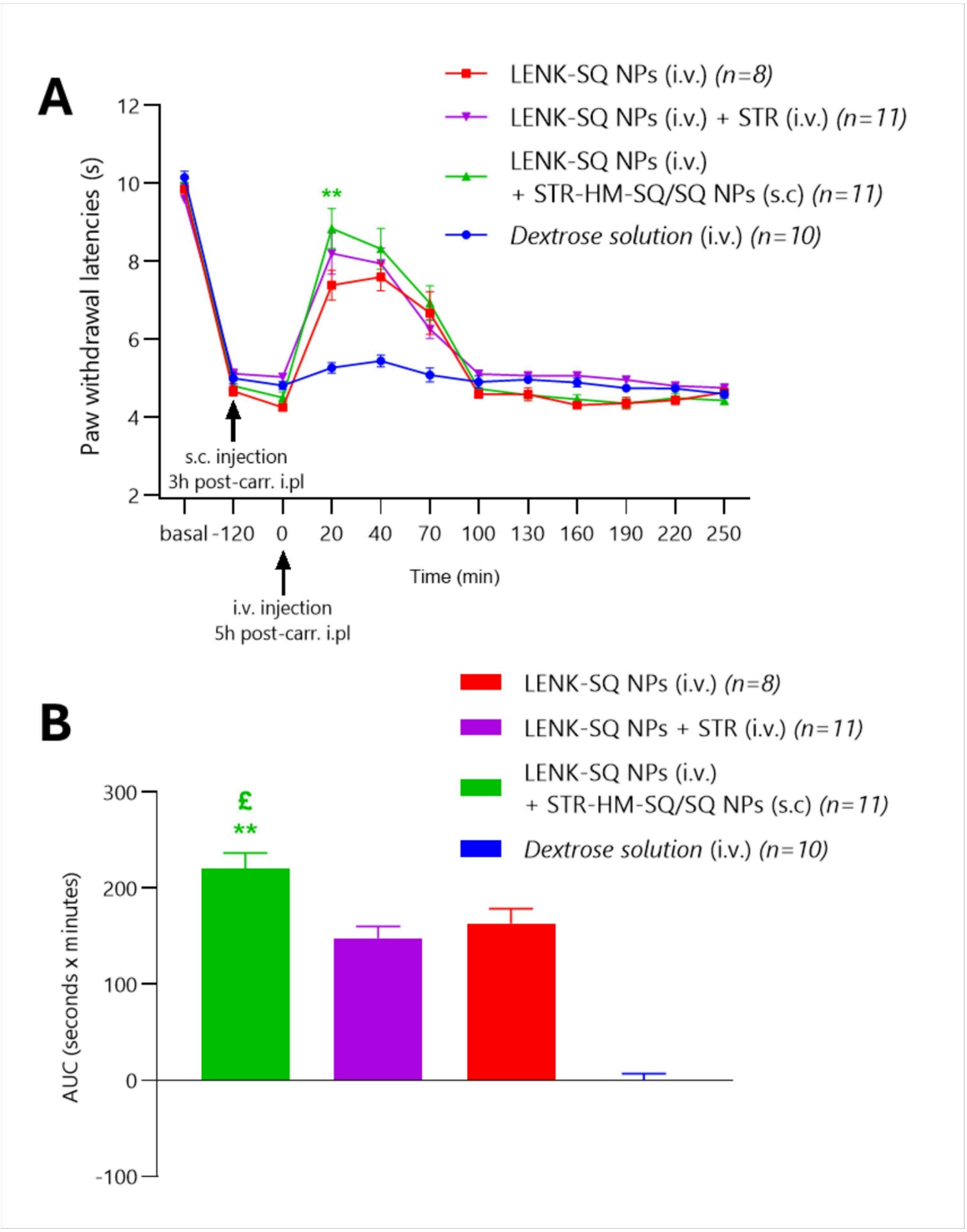

Figure 6

Anti-hyperalgesic activity of LENK-SQ NPs (i.v), LENK-SQ NPs + STR (i.v.) (*results from Fig. 1)*, and LENK-SQ NPs + STR-HM-SQ/SQ NPs (s.c.) in comparison with dextrose solution (vehicle) in a carrageenan-induced inflammatory pain in rats. Subcutaneous administration of STR-HM-SQ NPs was performed on the back of the rat (green arrow, -120 on x-axis) 3 hours after carrageenan injection into the left hind paw.

Administration of all other treatments was performed (arrow, 0 on x-axis) 5 hours after intraplantar injection of carrageenan **(A)** Subcutaneous injection of STR-HM-SQ/SQ NPs combined with the intravenous administration of LENK-SQ NPs resulted in an increased paw withdrawal latency, at 20 min (in seconds, means ± SEM of independent determinations), as measured by the Hargreaves test, compared to LENK-SQ NPs alone (P= 0,003). Two-way analysis of variance (ANOVA) with repeated measures, Bonferroni post-test. **(B)** Bars represent the means ± SEM of AUCs (seconds x minutes) for the cumulative anti-nociceptive durations, derived from the time course changes in PWL after the various treatments. P=0.0278 compared to LENK-SQ NPs; P=0.001 compared to the combination of LENK-SQ NPs with STR. One-way ANOVA, Tukey post-test. Raw data are shown in table SI-1.

Supplementary Files

This is a list of supplementary files associated with this preprint. Click to download.

- Graphicalabstract.png
- SupplementaryInformationDDTR.docx